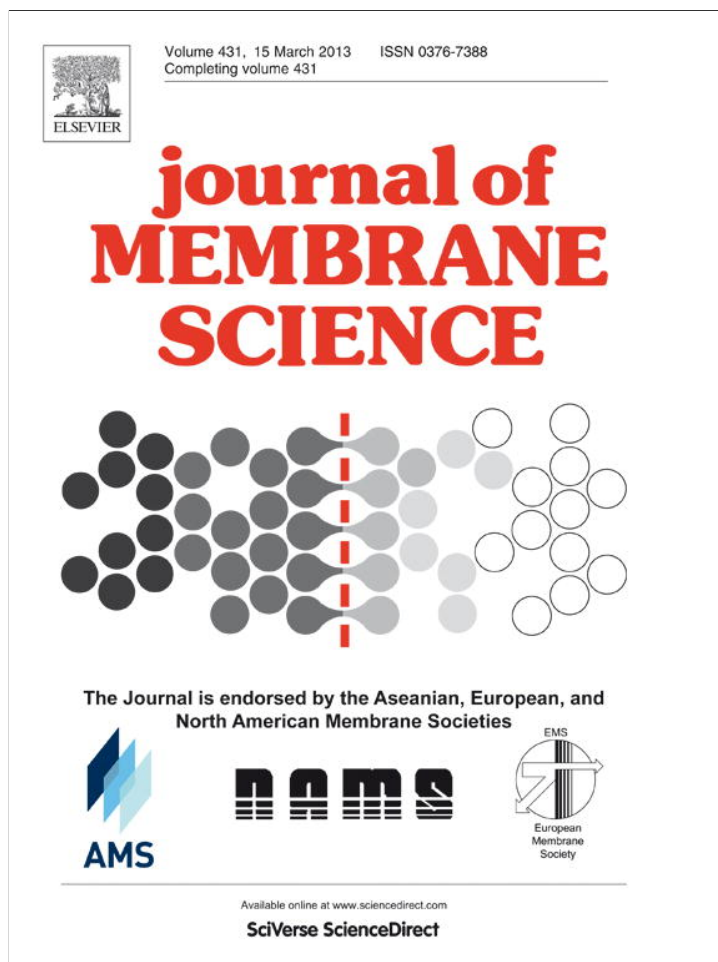


Provided for non-commercial research and education use.  
Not for reproduction, distribution or commercial use.



This article appeared in a journal published by Elsevier. The attached copy is furnished to the author for internal non-commercial research and education use, including for instruction at the authors institution and sharing with colleagues.

Other uses, including reproduction and distribution, or selling or licensing copies, or posting to personal, institutional or third party websites are prohibited.

In most cases authors are permitted to post their version of the article (e.g. in Word or Tex form) to their personal website or institutional repository. Authors requiring further information regarding Elsevier's archiving and manuscript policies are encouraged to visit:

<http://www.elsevier.com/copyright>

Contents lists available at [SciVerse ScienceDirect](http://www.sciencedirect.com)

## Journal of Membrane Science

journal homepage: [www.elsevier.com/locate/memsci](http://www.elsevier.com/locate/memsci)

## Direct microscopic observation of membrane formation by nonsolvent induced phase separation

Gregory R. Guillen<sup>a,b</sup>, Guy Z. Ramon<sup>a,b,1</sup>, H. Pirouz Kavehpour<sup>c</sup>, Richard B. Kaner<sup>b,d</sup>, Eric M.V. Hoek<sup>a,b,\*</sup>

<sup>a</sup> Department of Civil & Environmental Engineering, University of California, Los Angeles, Los Angeles, California, USA

<sup>b</sup> California NanoSystems Institute, University of California, Los Angeles, Los Angeles, California, USA

<sup>c</sup> Department of Mechanical and Aerospace Engineering, University of California, Los Angeles, Los Angeles, California, USA

<sup>d</sup> Department of Chemistry and Biochemistry, University of California, Los Angeles, Los Angeles, California, USA

### ARTICLE INFO

#### Article history:

Received 25 September 2012

Received in revised form

11 December 2012

Accepted 13 December 2012

Available online 1 January 2013

#### Keywords:

Phase inversion

Polysulfone

Filtration

Membrane morphology

Macrovoids

### ABSTRACT

Membrane formation by nonsolvent induced phase inversion was directly observed using light microscopy. Polysulfone (PSF) was used as a model polymer while 1-methyl-2-pyrrolidinone (NMP), *N,N*-dimethylformamide (DMF), water and glycerol were used as model solvents and nonsolvents. Direct observation and kinetic analyses suggest finger-like macrovoids formed by convective flow of nonsolvent into the polymer–solvent solution; convective flow arose from interfacial energy gradients at the polymer solution–nonsolvent interface. Convective nonsolvent flow into the polymer solution was hindered by the formation of surface skin layers or viscous gel layers within the polymer solution film. Viscous gel layers were often formed when using a poor nonsolvent, poor solvent, or an insufficient supply of a good nonsolvent. Greater viscous hindrance resulted in membranes with shorter or no finger-like macrovoids. Large finger-like macrovoids propagated only when nonsolvent convective flows into the polymer solution film exceeded viscous hindrance forces, i.e., when a good solvent, ample supply of good nonsolvent, and polymer solution of relatively lower viscosity were used.

© 2012 Elsevier B.V. All rights reserved.

### 1. Introduction

Nonsolvent induced phase inversion is a process by which a polymeric membrane can be formed with an asymmetric structure. A polymer is dissolved in a good solvent (“solvent”). A poor solvent (“nonsolvent”) is chosen that is generally miscible with the solvent. Contacting the polymer solution (generally polymer + solvent) with nonsolvent causes the polymer to precipitate due to solvent–nonsolvent exchange [1–6]. A number of mechanisms have been proposed to describe membrane formation during nonsolvent induced phase inversion. Interfacial hydrodynamic instabilities induced by surface tension gradients have been suggested as the cause of macrovoid initiation [4,7–9]. Macrovoid formation has been linked to excess intermolecular potential gradients due to the concentration gradients at the polymer solution–nonsolvent bath interface [10]. Boom et al. and Smolders et al. claimed that macrovoid formation stemmed from nucleation

of the polymer-poor phase and propagated as long as the polymer solution ahead of the voids remained stable for a sufficient time. Voids grew as solvent diffused from the polymer-rich phase into the polymer-poor phase [11,12].

The state of the polymer solution prior to immersion into the coagulation bath is critical in determining the final membrane morphology. Finger-like macrovoid formation can be suppressed by increasing polymer concentration in the polymer solution [7,9,13–18], increasing solvent evaporation time [7,16,19], adding solvent to the coagulation bath [6,20–22], adding nonsolvent to the polymer solution [7,11,17–19,21,23–26], introducing organic additives such as polyvinylpyrrolidone to the polymer solution [12,27], or by choosing a solvent/nonsolvent pair with low miscibility [7,22,23]. Macrovoid formation in hollow fiber membranes can be suppressed by increasing elongation draw ratio [28].

The work by Matz has led the way for the direct observation of film formation by phase inversion [8,9]. Generally, a drop of polymer solution is spread thin between glass slides and contacted with a nonsolvent. The phase inversion process is then observed through a light microscope. Frommer and Messalem used this method to provide evidence for macrovoid growth by convective flows within the polymer solution film [7]. Strathmann et al. used direct observation of phase inversion to find that high precipitation rates lead to membranes with large finger-like macrovoids, while a slow precipitation rate lead to membranes with

\* Correspondence to: University of California, Los Angeles, 5732 Boelter Hall, PO Box 951593, Los Angeles, CA 90095-1593, United States. Tel.: +1 310 206 3735; fax: +1 310 206 2222.

E-mail address: [emvhoek@ucla.edu](mailto:emvhoek@ucla.edu) (E.M.V. Hoek).

<sup>1</sup> Current address: Department of Mechanical and Aerospace Engineering, Princeton University, Princeton, New Jersey 08540, USA.

sponge-like structures [20]. The slow precipitation rate was attributed to retardation by a viscous sublayer ahead of the precipitating polymer front. This visualization technique continues to be used and has proven to be a valuable tool in understanding phase inversion membrane formation mechanisms [29–32]. This technique suffers from a few shortcomings. It can be difficult to maintain a constant film thickness between glass slides. The diameter of a spread polymer solution drop (millimeters) is often much greater than the thickness typical of membrane casting (hundreds of micrometers). The greater distance and volume between the spread polymer solution drop–nonsolvent interface and drop center may provide an inordinately large supply of solvent and may affect phase inversion. It is difficult to observe film formation in opaque polymer solutions. This technique does, however, allow for the real time measurement of void formation and uses only a small amount of material, so it may be used to rapidly evaluate novel polymer–solvent–additive–nonsolvent combinations.

Herein, we directly observe film formation for PSf polymer solutions containing the commonly-used solvents NMP and DMF along with water and glycerol as nonsolvents. The relationship between polymer, solvent, nonsolvent, and formation conditions on membrane morphology will be discussed for polymer–solvent–nonsolvent systems comprising PSf–NMP–water, PSf–DMF–water, and PSf–NMP–water/glycerol.

## 2. Materials and methods

### 2.1. Materials

Ultra-pure 18 M $\Omega$  deionized (DI) water was produced by a reverse osmosis system (RODI-C-12BL, Aqua Solutions, Inc.). NMP (Sigma-Aldrich, no. 443778), DMF (Sigma-Aldrich, no. 319937), glycerol (Sigma-Aldrich, no. W252506), and PSf beads (Sigma-Aldrich, no. 182443,  $M_n \sim 22$  kDa) were all used as received. PSf polymer solutions were prepared by adding all PSf beads to the solvent while stirring rapidly in a tightly sealed glass vial. Solutions were allowed to stir for at least 3 days at room temperature.

### 2.2. Phase inversion visualization

Visualization of the phase inversion process was performed as described by Matz [8]. A polymer solution drop ( $\sim 10$   $\mu$ l) was placed between a glass slide and cover slip. Drops were spread and thinned using the cover slip. A drop of nonsolvent was added to the edge of the cover slip in order to contact the polymer solution. Relative humidity varied between 40–50% during phase inversion visualization. The phase inversion process was observed using an optical microscope (Olympus BX51WI, Japan) employing a 40 $\times$  objective lens and recorded using a digital camera (Fujifilm FinePix F60fd, Japan) at 3 $\times$  optical zoom. Video was recorded at 25 frames/s. Void growth rates were determined with the aid of Phantom tracking software ver. 8.4.630 (Vision Research, Inc., USA) in conjunction with a hemacytometer (Bright-Line<sup>TM</sup>). Void geometry was determined using NIH ImageJ software.

### 2.3. Membrane formation

Membranes were formed by immersion precipitation [33]. Polymer solutions were left to stand sealed for 1 h before film casting. Films were spread using a casting knife (Gardco Adjustable Micrometer Film Applicator, Microm II, AP-99500701) with a blade height of 152  $\mu$ m set using a feeler gauge. Films were hand-cast on a glass plate and immediately placed in a coagulation bath containing 3 l of DI water at 20  $^{\circ}$ C. Relative humidity during film casting was 50–55%. Membranes remained in the coagulation bath for 30 min before transferring to plastic storage bags containing DI water. Water in the storage bags was replaced with fresh DI water every 30 min for 2 h. Membranes were then stored at 4  $^{\circ}$ C in DI water prior to further characterization.

### 2.4. SEM sample preparation

Membrane cross-sections were prepared from unsupported films by freeze fracturing using liquid nitrogen. Samples were then dried in a desiccator overnight at 20  $^{\circ}$ C before sputter-coating with gold to prevent charging. Membrane cross-sections were mounted vertically for SEM imaging using a Nova 600 NanoLab DualBeam<sup>TM</sup>-SEM/FIB (FEI Company, Hillsboro, Oregon, USA).

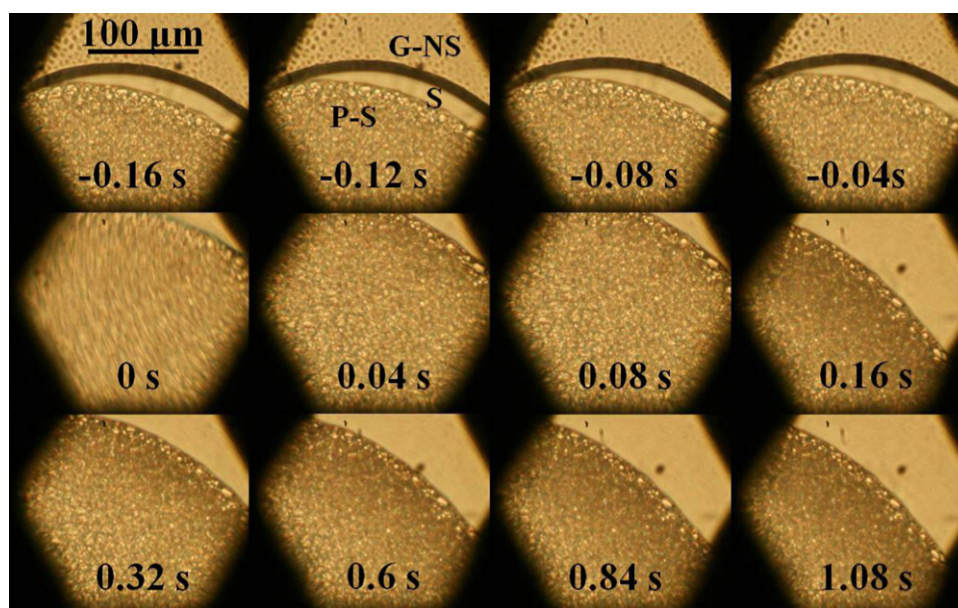


**Fig. 1.** Time sequence images of the formation of sponge-like morphology in 18 wt% PSf–82 wt% DMF–water system. Region P–S is the polymer solution drop, S is solvent, and G–NS is gas for  $t < 0$  s and nonsolvent for  $t \geq 0$  s.

### 3. Results and discussion

#### 3.1. PSf-DMF–water system

An 18 wt% PSf polymer solution was prepared using DMF as the solvent. The phase inversion process was visualized using DI water at 20 °C as the nonsolvent. A set of time sequence images of this process is shown in Fig. 1. The polymer and solvent begin to separate as soon as the polymer solution drop is placed on the glass slide and prior to the introduction of a nonsolvent drop. Region “P-S” appears to be composed of PSf and DMF and has begun phase separation. Small droplets containing higher concentrations of PSf are easily observed. Region P-S remains fluid despite the initiation of phase separation. The clear layer above region P-S, region “S”, appears to be composed of DMF that has been expelled

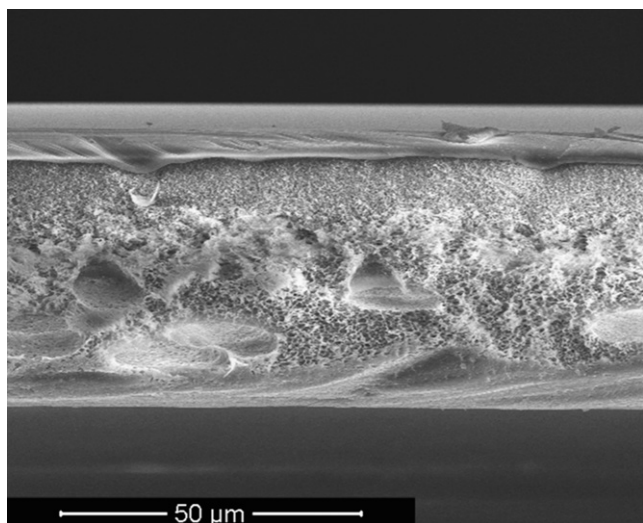


Fig. 2. SEM cross-section image of 18 wt% PSf-82 wt% DMF membrane showing sponge-like morphology.

from the polymer solution drop by syneresis, i.e., DMF has been locally squeezed out of region P-S as it shrinks. The rapid destabilization of the PSf-DMF polymer solution is potentially due to the laboratory relative humidity (40–50%) during the visualization experiments. Cloud point data for the PSf-DMF–water system show that only a small amount of water (1–2 wt%) is required to induce phase separation [34]. Similar observations were described by Han et al. [34] in which they noted that DMF is nonvolatile and highly hygroscopic. The polymer solution drop is contacted with a nonsolvent drop from region G-NS at time=0 s. Upon nonsolvent addition, the polymer solution drop contracts and the polymer-rich phase becomes visually denser. This is likely due to the additional expulsion of DMF with limited water uptake. The darker polymer-rich phase indicates that PSf has precipitated. The PSf-DMF–water system produces a sponge-like morphology free of finger-like macrovoids. Although it is difficult to track the rate of polymer precipitation using this visualization method, the polymer-rich phase is shown to reach its ultimate morphology during a time scale on the order of 1 s.

A scanning electron micrograph of a cross-section of a hand-cast 18 wt% PSf-82 wt% DMF membrane formed using DI water at 20 °C is presented in Fig. 2. The laboratory relative humidity during casting of this membrane was 50–55%. This membrane has a sponge-like morphology, which is free of finger-like macrovoids. The morphology of the freeze-fractured, hand-cast PSf-DMF membrane is very similar to that shown in the time sequence images (Fig. 1). The average film thickness of this membrane was determined from image analysis (NIH ImageJ software) to be 40 μm.

#### 3.2. PSf-NMP–water system

An 18 wt% PSf polymer solution was prepared using NMP as the solvent. The phase inversion process, using DI water at 20 °C as the nonsolvent, was visualized. A set of time sequence images of this process is shown in Fig. 3. The polymer and solvent are stable prior to the introduction of the nonsolvent drop. Region P-S

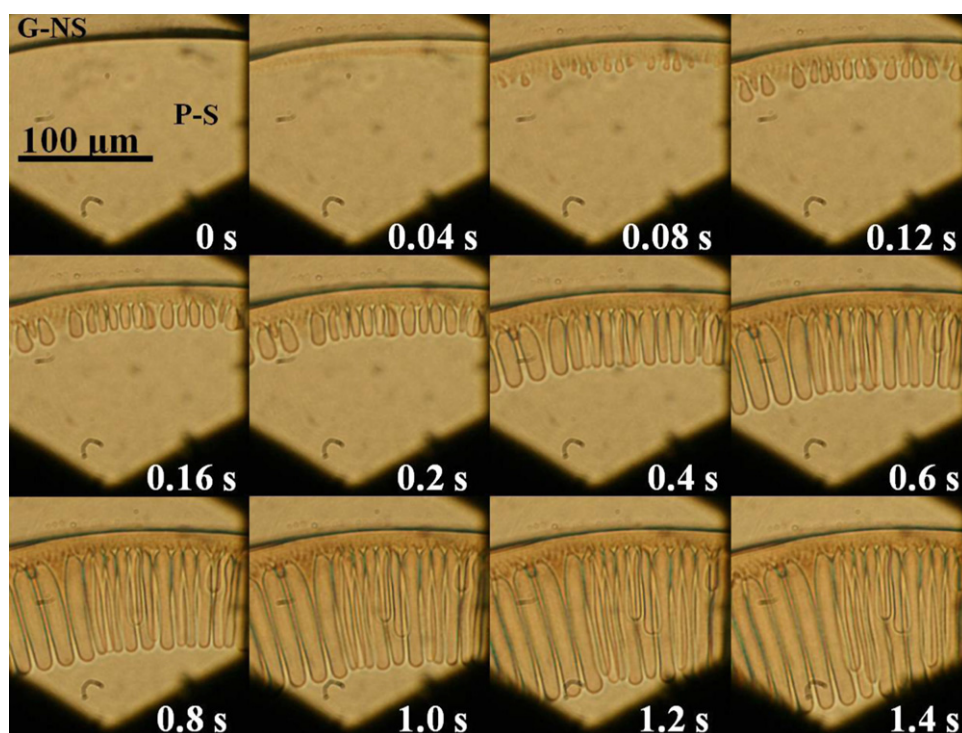


Fig. 3. Time sequence of void formation in 18 wt% PSf-82 wt% NMP–water system. Region P-S is the polymer solution drop and region G-NS is the nonsolvent.

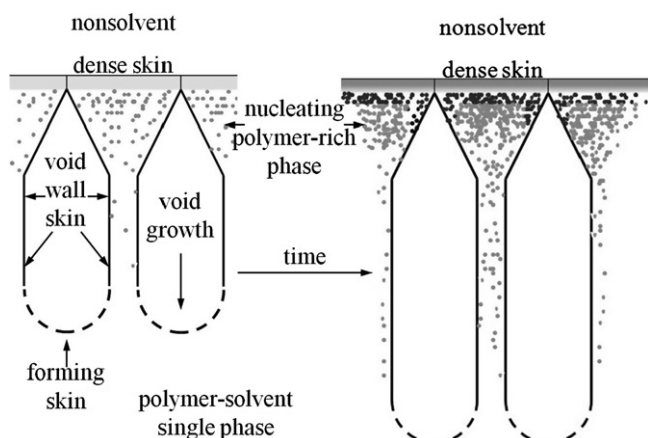


Fig. 4. Illustration of finger-like void formation.

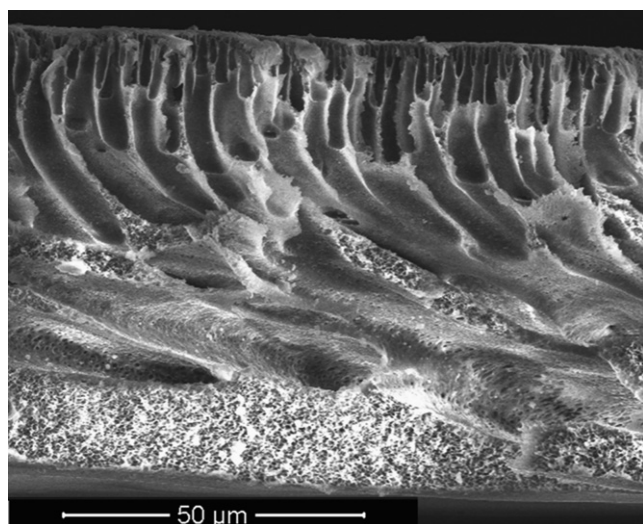


Fig. 5. SEM cross-section image of 18 wt% PSf-82 wt% NMP membrane showing sponge-like morphology between finger-like macrovoids.

is a single, fluid phase composed of PSf and NMP. The polymer solution drop is contacted with a nonsolvent drop introduced from region G-NS at time  $t=0$  s. Finger-like macrovoids form upon addition of nonsolvent. Faint traces of the beginnings of voids are observed within the first 40 ms, and the voids grow to 100  $\mu\text{m}$  in length within  $\sim 1$  s. Finger-like voids grow directionally from the polymer solution–nonsolvent interface toward the drop center.

Cloud point data for the PSf-NMP–water system show that the presence of a small amount of water ( $\sim 4$  wt%) is enough to induce phase separation [35]. Unlike the PSf-DMF polymer solution, however, the PSf-NMP polymer solution remains stable as a single phase until a nonsolvent drop is added. Hansen solubility parameters have been commonly used as a tool for predicting polymer solubility. Hansen solubility theory states that the total energy of vaporization of a solvent is composed of (atomic) dispersion forces, (molecular) permanent dipole–permanent dipole forces, and (molecular) hydrogen bonding forces [36]. Polymers and solvents with similar Hansen solubility parameters will have a high mutual affinity. Solvent–polymer affinity is quantified by a solvent–polymer pair’s relative energy difference (RED). Polymer–solvent  $\text{RED} < 1$  indicates that the polymer is likely soluble in the given solvent. Lower RED values indicate greater polymer–solvent compatibility.  $\text{RED} > 1$  indicates that the polymer is likely to be insoluble in the given solvent. Hansen solubility parameters predict NMP to be a better solvent for PSf than DMF, with REDs for PSf-NMP and PSf-DMF of 0.67 and 0.96, respectively [33,36]. Once water is introduced into a polymer solution, DMF partitions into a polymer-poor phase in a PSf-DMF drop/film more readily than NMP in a PSf-NMP drop/film. The PSf-NMP–water system produces both finger-like macrovoids and sponge-like morphologies. An illustration of void formation for the 18 wt% PSf-82 wt% NMP–water system is shown in Fig. 4.

Polymer precipitation occurs instantly at the polymer solution–nonsolvent interface, where solvent–nonsolvent exchange is the most rapid, but is hindered below this nascent surface skin layer due to a higher local concentration of NMP. During phase separation and finger formation in the PSf-NMP–water system, the region between finger-like voids is initially fluid. Polymer precipitation also occurs rapidly at the inner walls of the finger-like voids and forms a thin skin. This acts to reinforce the void’s shape. The leading front of the finger-like void remains relatively fluid as long as the

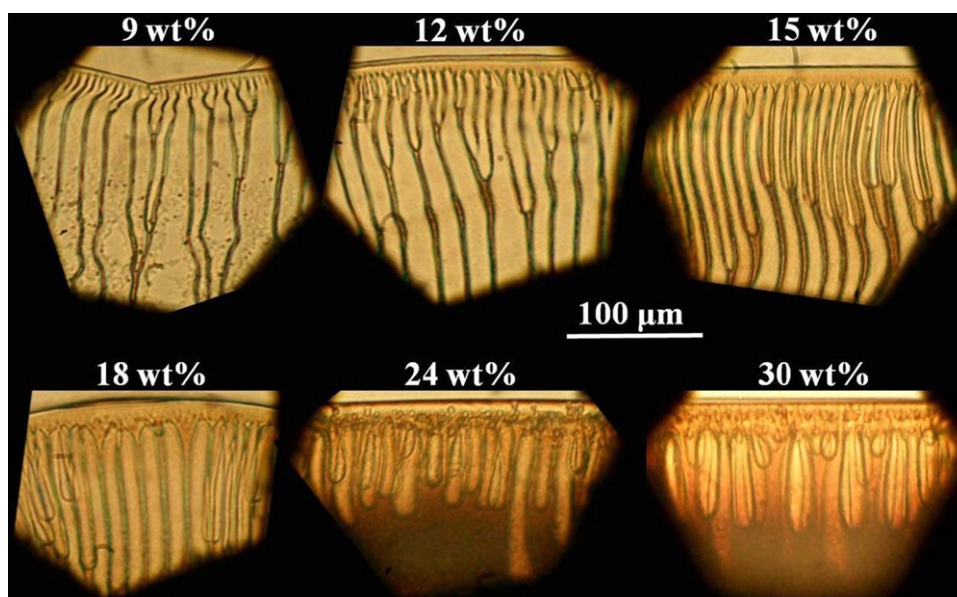


Fig. 6. Images of PSf-NMP films with varying PSf wt%.

water penetration is of sufficient rate. Water slowly diffuses into the inter-void regions of the membrane either through the dense skin layer at the membrane surface or through the skinned void walls. The precipitated polymer skin layers and the dilutive effects of the solvent hinder solvent–nonsolvent exchange. The gradual influx of water into the inter-void region of the film causes nucleation of the polymer-rich phase and eventually polymer precipitation. The PSf-NMP–water membrane morphology between the finger-like macrovoids is similar to that of the PSf-DMF–water membrane bulk morphology; a sponge-like morphology arises from precipitated nuclei formed by hindered nonsolvent influx.

A scanning electron micrograph of a cross-section of a hand-cast 18 wt% PSf-82 wt% NMP membrane formed using DI water at 20 °C is presented in Fig. 5. This membrane has finger-like macrovoids with sponge-like morphology in the inter-void regions. The morphology of the freeze-fractured, hand-cast PSf-NMP membrane is very similar to that shown in the time sequence images (Fig. 3). The average film thickness of this membrane was determined from image analysis to be 74 μm.

### 3.2.1. Variable polysulfone wt%

Polysulfone wt% was varied from 9–30 wt% using NMP as the solvent and DI water at 20 °C as the nonsolvent. Images of ultimate membrane morphology are shown in Fig. 6. These images were analyzed for void number density, skin thickness, average void width, and ultimate void length. Each membrane morphology parameter is plotted in Fig. 7. Void number density is expressed as the number of voids counted per 100 μm on a line approximately 20 μm below and parallel to the film/nonsolvent

interface. Skin thickness is measured as the distance between the film/nonsolvent interface and the initiation point of the voids. Ultimate void length is measured as the average void penetration distance from the film/nonsolvent interface into the polymer solution drop. This was determined from image analysis of 10 × magnification video scans of voids within the precipitated polymer solution drops.

Void number density remains relatively constant with PSf wt%. Average void width is a minimum at 15 wt% PSf and varies by a factor of 2. Skin thickness increases linearly with increasing PSf wt%. Ultimate void length decreases exponentially with increasing PSf wt%. The 9 wt% PSf polymer solution produced finger-like macrovoids upwards of 6 mm in length, while the 30 wt% PSf polymer solution produced finger-like macrovoids 0.2 mm in length.

Void growth rate was measured in real time for PSf-NMP polymer solutions of varying PSf wt% and the results are shown in Fig. 8. Voids grow to 100 μm in length on the order of ~1 s for the PSf-NMP–water system (Fig. 8(a)). When void length is plotted against  $t^{1/2}$ , a fairly linear relationship is observed (Fig. 8(b)). Void growth rate can be expressed as an apparent diffusion coefficient,  $D=x^2/t$ , where  $x$  is some distance into the polymer solution, and  $t$  is the time for a finger-like void to grow to length  $x$ . The apparent diffusion coefficients at  $x=50$  μm into the film for all PSf wt% tested are shown in Fig. 9. The apparent diffusion coefficients are between 2–4 times that of the mutual diffusion coefficient of water ( $D_0=2.2 \times 10^{-9}$  m<sup>2</sup>/s) [37]. Finger-like void formation rate exceeds the rate of water diffusion into the film. This finding is in agreement with previous results of high apparent diffusion coefficients in films with finger-like voids [20].

### 3.2.2. Initiation of a surface gel layer

Another 18 wt% PSf polymer solution was prepared using NMP as the solvent. The phase inversion process was visualized using

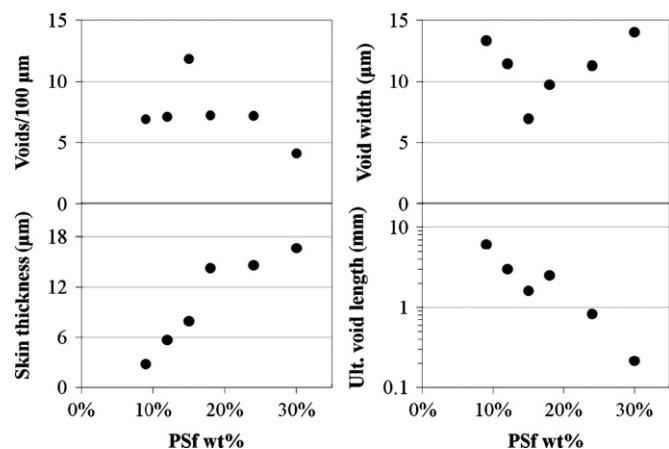


Fig. 7. Void characteristics of PSf-NMP films with varying PSf wt%.

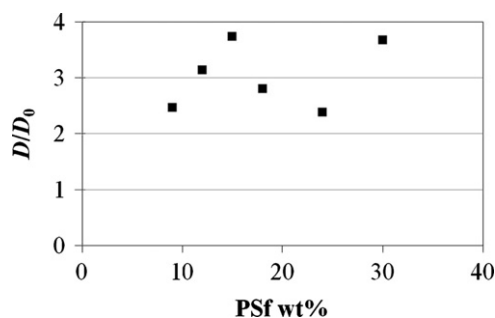


Fig. 9. Normalized apparent diffusion coefficient for PSf-NMP–water system.

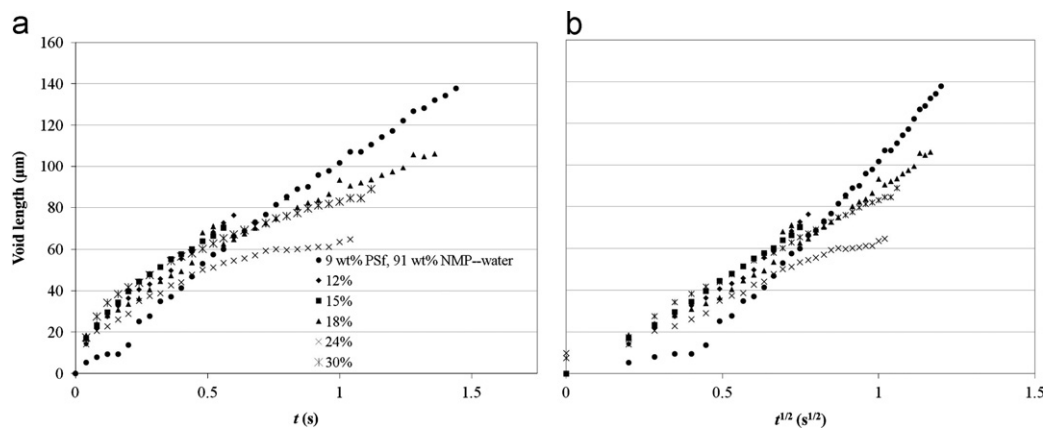
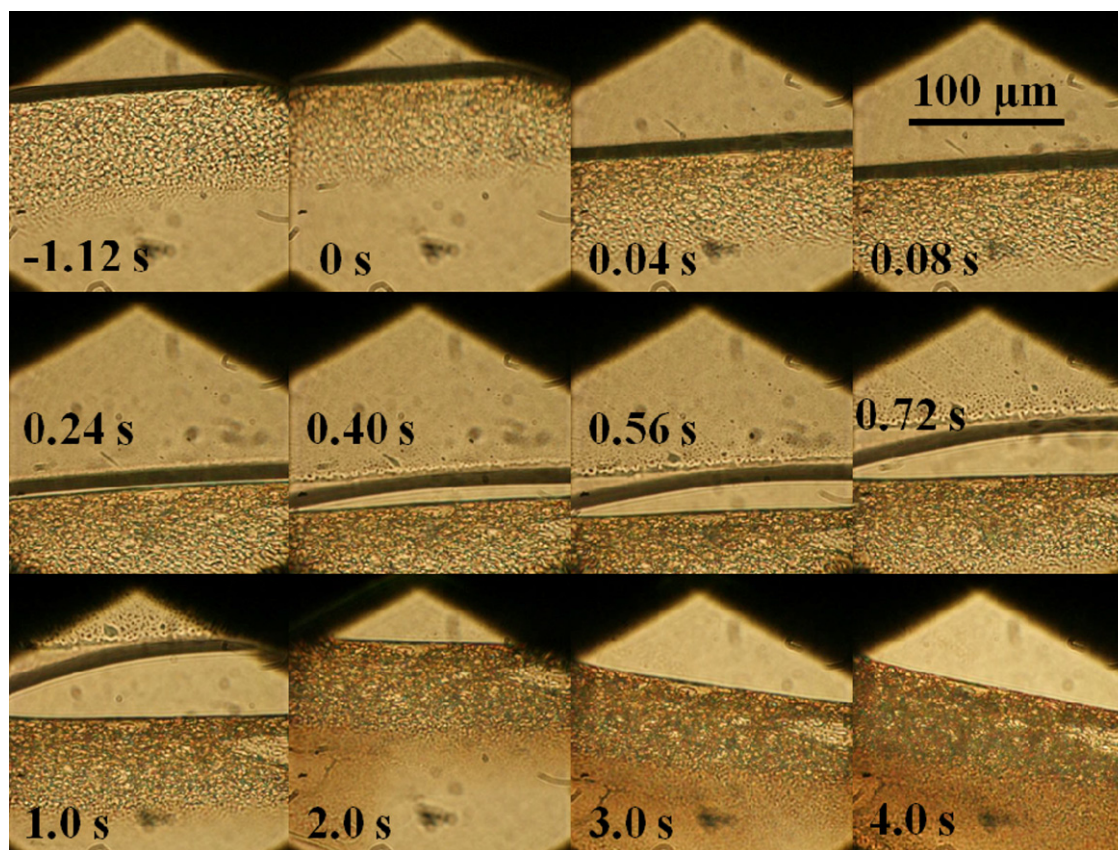


Fig. 8. Void growth rates for PSf-NMP–water system of varying PSf wt% plotted against time (a) and  $t^{1/2}$  (b).



**Fig. 10.** Time sequence images of dense film formation in 18 wt% PSF-82 wt% NMP–water system where the surface of the polymer solution has imbibed a small amount of water prior to immersion in nonsolvent.

DI water at 20 °C as the nonsolvent. A set of time sequence images of this process is shown in Fig. 10. Here, the polymer and solvent are unstable prior to the introduction of the nonsolvent drop. This is achieved by spreading the polymer solution drop over a glass slide covered with a small amount of residual water. Small amounts of nonsolvent contact the outer edge of the spreading polymer solution drop. This gradual and localized introduction of nonsolvent causes nucleation of the polymer-rich phase near the outer edge of the polymer solution drop. This destabilized two-phase outer edge region and the single-phase region below are both initially fluid. The two-phase outer edge region appears to be more viscous than the single-phase interior region. The polymer solution drop is contacted with a nonsolvent drop at time=0 s. The film precipitates in a very similar manner to the PSF-DMF–water system. A sponge-like structure is formed without large voids. The presence of a viscous gel layer at the drop outer edge region inhibited the formation of large finger-like voids.

This process of gradual and local destabilization of the polymer solution is similar to vapor induced phase inversion where nonsolvent vapor is used to coagulate the polymer solution [29,32,38,39]. Park et al. found that films with a sponge-like structure could be formed from 15 wt% PSF-85 wt% NMP polymer solutions by precipitating with water vapor [32]. They found that finger-like voids were not formed when relative humidity was greater than 65–70%. The formation of a thin liquid layer above the phase-separated polymer solution seen in Fig. 10 has also been observed by Menut et al. who stated that the liquid layer is likely polymer solution expelled by syneresis [29]. This phenomena was observed during film formation in the PSF-DMF–water system (Fig. 1). A gradual and limited supply of nonsolvent to the polymer solution surface acts to destabilize the surface layer,

which produces a more viscous two-phase barrier to additional nonsolvent transport into the film.

Tiraferri et al. have shown the formation of large finger-like voids in a 9 wt% PSF-91 wt% DMF film precipitated using DI water [40]. They attributed the presence of finger-like voids to the relatively low viscosity of the polymer solution. We believe that this is partly true. The cloud point of this polymer solution is likely sufficiently high so that the atmospheric relative humidity did not provide enough water into the surface layer of the polymer solution film to cause nucleation of the polymer-rich phase. In this case, resistance to void formation by a viscous surface layer was insufficient to prevent finger-like void formation. We further hypothesize that finger-like macrovoids can be formed in other PSF-DMF polymer solutions provided that these films are cast in a dry environment prior to immersion in a nonsolvent bath.

### 3.2.3. Void growth by convective nonsolvent flows dampened by polymer solution viscosity

Mass transfer through liquid interfaces is often associated with large convective flows near the interface [7,41–46]. Frommer and Messalem suggested that the formation of large finger-like macrovoids in polymer solutions are caused by convective flows [7]. Gradients in density and/or interfacial energy are the driving forces for convective flows near liquid interfaces [41–46]; hence, they ruled out density gradients as a mechanism for the formation of finger-like macrovoids by immersing polymer solution films in coagulation baths in both upward-facing and downward-facing orientations. Voids formed irrespective of film orientation [7]. This result is confirmed here where polymer

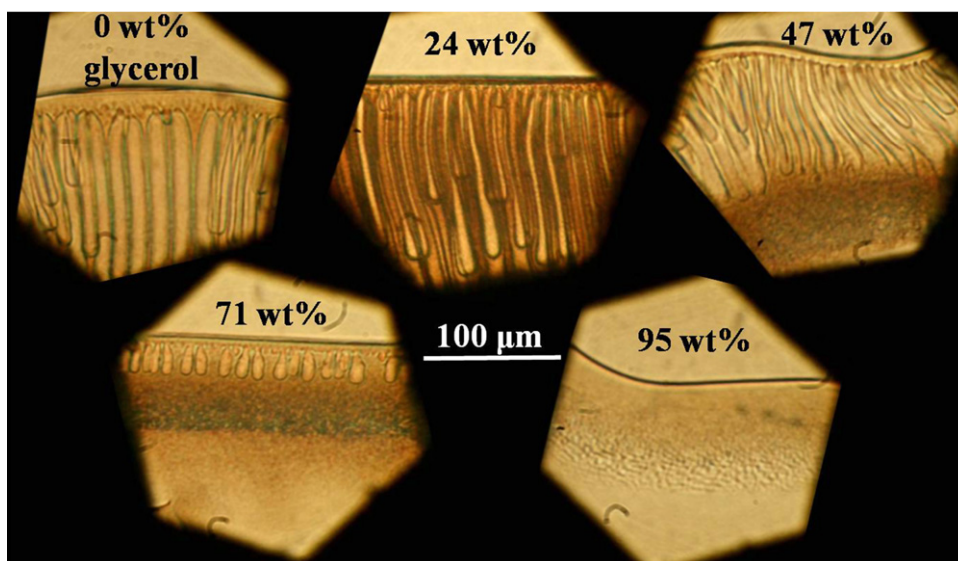


Fig. 11. Images of 18 wt% PSf-82 wt% NMP films with varying glycerol–water content mixtures used as the nonsolvent.

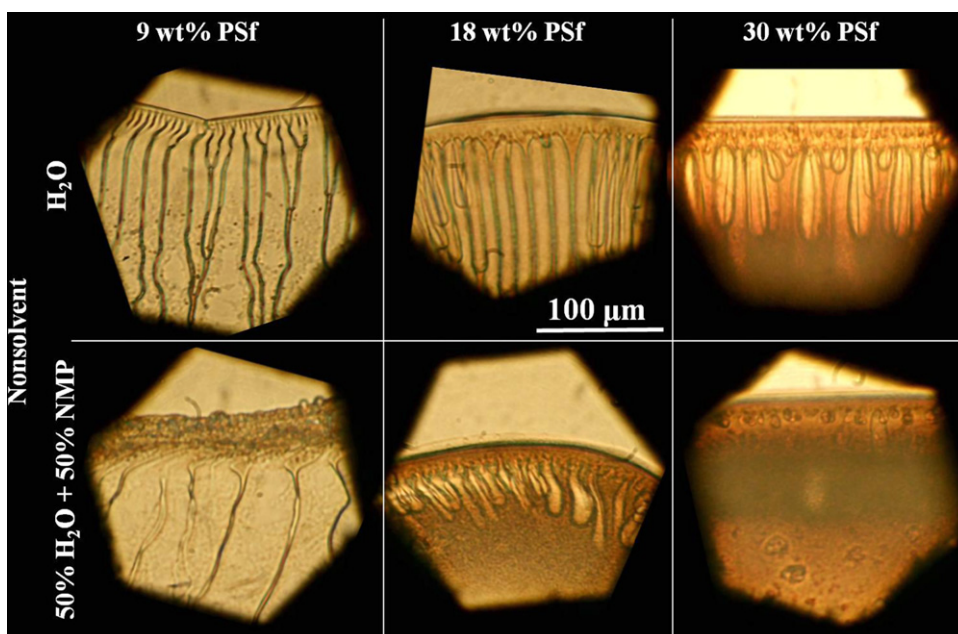


Fig. 12. Images of PSf-NMP films with water and water-NMP mixtures used as the nonsolvent.

solution and nonsolvent were contacted in a plane perpendicular to gravity with void formation within this plane. This leaves gradients in interfacial energy as the remaining driving force for the initiation of convective flows near the polymer solution-coagulation bath interface. Further indication of such a mechanism may be found in noting that a  $t^{1/2}$  scaling is typical of viscous (damped) meniscus propagation in capillary imbibition [47]. Frommer and Messalem stated that once convective flows are initiated they may be enhanced or dampened by changes in concentration, temperature, viscosity, etc. [7]. An increase in polymer solution viscosity hinders the extent of large void formation. Increasing bulk polymer solution concentration, and therefore polymer solution viscosity, hinders finger-like macrovoid formation (see Fig. 7). Increasing polymer solution viscosity locally at the polymer solution-coagulation bath interface by creating a gel layer due to solvent evaporation or by destabilizing the polymer solution by some other means greatly reduces the formation of large voids. It should be noted here that local

viscosity is merely a damping effect. The mechanism for void formation is convective flow of nonsolvent through the polymer solution, driven by gradients in interfacial energy. An adequate supply of nonsolvent must be in intimate contact with the polymer solution for convective flow. A limited supply of nonsolvent (e.g., water vapor) may be insufficient to drive convective flow and void formation.

#### 3.2.4. Nonsolvent quality

The quality of nonsolvent must also be considered. Water is an excellent nonsolvent for PSf, with an RED for PSf-water of 4.5. REDs for PSf-isopropanol, PSf-ethanol, and PSf-methanol are 1.4, 1.7, and 2.1, respectively [33,36]. The RED for PSf-glycerol is 2.7, which lies midway between the REDs of a suitable PSf solvent (1) and water (4.5), the best-known PSf nonsolvent. Images of 18 wt% PSf-82 wt% NMP films formed using glycerol–water solutions as the nonsolvent are shown in Fig. 11. Void length clearly

decreases with increasing glycerol content. Void formation is completely inhibited at a nonsolvent composition of 95 wt% glycerol. Nonsolvent viscosity, in addition to nonsolvent quality, may be a factor in void formation. Pure glycerol has a viscosity of 1.4 Pa·s at 20 °C, while water has a viscosity of  $1.0 \times 10^{-3}$  Pa·s at 20 °C [48]. Water (72 mN/m) and glycerol (64 mN/m) have similar surface tensions at 20 °C when compared to solvents NMP (41 mN/m) and DMF (37 mN/m) [49]. Void growth is inhibited when NMP is added to water to form a nonsolvent mixture. Adding NMP to water decreases its effectiveness as a nonsolvent. Images of 9, 18, and 30 wt% PSf polymer solutions with NMP as the solvent are shown in Fig. 12. Adding 50 wt% NMP to the nonsolvent water decreases finger-like void formation. There is still ample driving force for void formation for each polymer solution–nonsolvent combination. The higher polymer wt% solutions, however, are more viscous and dampen void penetration.

#### 4. Conclusions

Direct microscopic observation provides invaluable insight into the mechanisms of membrane formation by nonsolvent induced phase inversion. Mechanisms elucidated from preliminary studies suggest PSf membranes can be formed without finger-like macrovoids using both NMP and DMF, which may be of practical interest because NMP is an easier solvent to work with at industrial scale and macrovoids weaken membrane mechanical properties. Polymer solutions prepared in DMF take up enough water from atmospheric humidity to cause the polymer-rich phase to nucleate. Once the destabilized film is immersed in nonsolvent, the viscous nucleated phase at the surface of the film acts as a barrier to nonsolvent penetration and prevents finger-like macrovoid formation. Practically, this necessitates exquisite control over humidity of the membrane casting environment, which adds cost to membrane production. In contrast, polymer solutions prepared in NMP are generally less responsive to relative humidity because NMP, while somewhat hygroscopic like DMF, is a very good solvent for PSf. We find that slow addition of a good nonsolvent or rapid addition of a poor nonsolvent to the surface of a PSf-NMP film forms a skin that serves as a barrier against nonsolvent penetration (similar to the effect of atmospheric humidity on PSf-DMF solutions) and produces a sponge-like morphology, free of macrovoids.

#### Acknowledgments

The authors thank Dr. Noah Bodzin at the UCLA Nanolab for help with SEM analysis. Funding for this research was provided in part by Abraxis Bioscience (now CalCap Equity) (G.R.G., R.B.K., and E.M.V.H.), and the Vaadia-BARD Postdoctoral Fellowship Award no. FI-435-2010 from BARD, The United States—Israel Binational Agricultural Research and Development Fund (G.Z.R.).

#### References

- [1] M. Mulder, *Basic Principles of Membrane Technology*, Kluwer Academic Publishers, Dordrecht, The Netherlands, 2003.
- [2] R.E. Kesting, *Synthetic Polymeric Membranes: A Structural Perspective*, Wiley-Interscience, New York, NY, 1985.
- [3] S. Manjikian, S. Loeb, J.W. McCutchan, in: *Proceedings of the First International Symposium on Water Desalination*, Washington, DC, 1965, pp. 251–274.
- [4] M.A. Frommer, D. Lancet, The mechanism of membrane formation: membrane structures and their relation to preparation conditions, in: H.K. Lonsdale, H.E. Podall (Eds.), *Reverse Osmosis Membrane Research*, Plenum Press, New York, 1972, p. 85.
- [5] M. Guillotin, C. Lemoyne, C. Noel, L. Monnerie, Physicochemical processes occurring during formation of cellulose diacetate membranes—research of criteria for optimizing membrane performance—4. Cellulose diacetate-acetone-organic additive casting solutions, *Desalination* 21 (1977) 165–181.
- [6] D.M. Koenhen, M.H.V. Mulder, C.A. Smolders, Phase separation phenomena during formation of asymmetric membranes, *J. Appl. Polym. Sci.* 21 (1977) 199–215.
- [7] M.A. Frommer, R.M. Messalem, Mechanism of membrane formation. 6. Convective flows and large void formation during membrane precipitation, *Ind. Eng. Chem. Prod. Res. Dev.* 12 (1973) 328–333.
- [8] R. Matz, Hydronautics, inc., quarterly progress report 7005-4 to the office of saline water, April 1970.
- [9] R. Matz, The structure of cellulose-acetate membranes 1. Development of porous structures in anisotropic membranes, *Desalination* 10 (1972) 1–15.
- [10] R.J. Ray, W.B. Krantz, R.L. Sani, Linear-stability theory model for finger formation in asymmetric membranes, *J. Membr. Sci.* 23 (1985) 155–182.
- [11] C.A. Smolders, A.J. Reuvers, R.M. Boom, I.M. Wienk, Microstructures in phase-inversion membranes 1. Formation of macrovoids, *J. Membr. Sci.* 73 (1992) 259–275.
- [12] R.M. Boom, I.M. Wienk, T. Vandenboomgaard, C.A. Smolders, Microstructures in phase inversion membranes 2. The role of a polymeric additive, *J. Membr. Sci.* 73 (1992) 277–292.
- [13] R.E. Kesting, A.K. Fritzsche, *Polymeric Gas Separation Membranes*, Wiley, New York, 1993.
- [14] S.S. Madaeni, A. Rahimpour, M. Barzin, Preparation of polysulphone ultra-filtration membranes for milk concentration: effect of additives on morphology and performance, *Iran. Polym. J.* 14 (2005) 421–428.
- [15] J. Barzin, S.S. Madaeni, H. Mirzadeh, M. Mehrabzadeh, Effect of polyvinylpyrrolidone on morphology and performance of hemodialysis membranes prepared from polyether sulfone, *J. Appl. Polym. Sci.* 92 (2004) 3804–3813.
- [16] F.G. Paulsen, S.S. Shojaie, W.B. Krantz, Effect of evaporation step on macrovoid formation in wet-cast polymeric membranes, *J. Membr. Sci.* 91 (1994) 265–282.
- [17] A. Bottino, G. Camera-Roda, G. Capannelli, S. Munari, The formation of microporous polyvinylidene difluoride membranes by phase-separation, *J. Membr. Sci.* 57 (1991) 1–20.
- [18] C. Friedrich, A. Driancourt, C. Noel, L. Monnerie, Asymmetric reverse-osmosis and ultrafiltration membranes prepared from sulfonated polysulfone, *Desalination* 36 (1981) 39–62.
- [19] L. Zeman, T. Fraser, Formation of air-cast cellulose-acetate membranes 1. Study of macrovoid formation, *J. Membr. Sci.* 84 (1993) 93–106.
- [20] H. Strathmann, K. Kock, P. Amar, R.W. Baker, The formation mechanism of asymmetric membranes, *Desalination* 16 (1975) 179–203.
- [21] J.M. Cheng, D.M. Wang, F.C. Lin, J.Y. Lai, Formation and gas flux of asymmetric PMMA membranes, *J. Membr. Sci.* 109 (1996) 93–107.
- [22] H. Strathmann, K. Kock, Formation mechanism of phase inversion membranes, *Desalination* 21 (1977) 241–255.
- [23] P. Neogi, Mechanism of pore formation in reverse-osmosis membranes during the casting process, *AIChE J.* 29 (1983) 402–410.
- [24] D.M. Wang, F.C. Lin, T.T. Wu, J.Y. Lai, Formation mechanism of the macrovoids induced by surfactant additives, *J. Membr. Sci.* 142 (1998) 191–204.
- [25] F.C. Lin, D.M. Wang, C.L. Lai, J.Y. Lai, Effect of surfactants on the structure of PMMA membranes, *J. Membr. Sci.* 123 (1997) 281–291.
- [26] Y.S. Kang, H.J. Kim, U.Y. Kim, Asymmetric membrane formation via immersion precipitation method 1. Kinetic effect, *J. Membr. Sci.* 60 (1991) 219–232.
- [27] R.M. Boom, T. Vandenboomgaard, C.A. Smolders, Mass-transfer and thermodynamics during immersion precipitation for a 2-polymer system—evaluation with the system PES–PVP–NMP–water, *J. Membr. Sci.* 90 (1994) 231–249.
- [28] K.Y. Wang, D.F. Li, T.S. Chung, S.B. Chen, The observation of elongation dependent macrovoid evolution in single and dual-layer asymmetric hollow fiber membranes, *Chem. Eng. Sci.* 59 (2004) 4657–4660.
- [29] P. Menut, Y.S. Su, W. Chinpa, C. Pochat-Bohatier, A. Deratani, D.M. Wang, P. Huguet, C.Y. Kuo, J.Y. Lai, C. Dupuy, A top surface liquid layer during membrane formation using vapor-induced phase separation (VIPS)—evidence and mechanism of formation, *J. Membr. Sci.* 310 (2008) 278–288.
- [30] J.S. Taurozzi, C.A. Crook, V.V. Tarabara, C(60)-polysulfone nanocomposite membranes: entropic and enthalpic determinants of C(60) aggregation and its effects on membrane properties, *Desalination* 269 (2011) 111–119.
- [31] X. Li, C. Chen, J. Li, Formation kinetics of polyethersulfone with cardo membrane via phase inversion, *J. Membr. Sci.* 340 (2009) 272–274.
- [32] H.C. Park, Y.P. Kim, H.Y. Kim, Y.S. Kang, Membrane formation by water vapor induced phase inversion, *J. Membr. Sci.* 156 (1999) 169–178.
- [33] G.R. Guillen, Y. Pan, M. Li, E.M.V. Hoek, Preparation and characterization of membranes formed by nonsolvent induced phase separation: a review, *Ind. Eng. Chem. Res.* 50 (2011) 3798–3817.
- [34] M.J. Han, P.M. Bummer, M. Jay, D. Bhattacharyya, Phase-transitions of polysulfone solution during coagulation, *Polymer* 36 (1995) 4711–4714.
- [35] J.Y. Kim, H.K. Lee, S.C. Kim, Liquid–liquid phase separation during polysulfone membrane preparation, *Korean J. Chem. Eng.* 17 (2000) 564–569.
- [36] C.M. Hansen, *Hansen Solubility Parameters—A User's Handbook*, 1st ed., CRC Press, Boca Raton, 2000.
- [37] J.P.C. Addad, B. Icard, L. Pellicoli, Skinned polymeric membranes—approach to the mechanism of formation of surface holes, *Polym. Int.* 38 (1995) 299–303.
- [38] J.T. Tsai, Y.S. Su, D.M. Wang, J.L. Kuo, J.Y. Lai, A. Deratani, Retainment of pore connectivity in membranes prepared with vapor-induced phase separation, *J. Membr. Sci.* 362 (2010) 360–373.

- [39] D. Bouyer, W. Werapun, C. Pochat-Bohatier, A. Deratani, Morphological properties of membranes fabricated by vips process using PEI/NMP/water system: SEM analysis and mass transfer modelling, *J. Membr. Sci.* 349 (2010) 97–112.
- [40] A. Tiraferri, N.Y. Yip, W.A. Phillip, J.D. Schiffman, M. Elimelech, Relating performance of thin-film composite forward osmosis membranes to support layer formation and structure, *J. Membr. Sci.* 367 (2011) 340–352.
- [41] J.C. Berg, C.R. Morig, Density effects in interfacial convection, *Chem. Eng. Sci.* 24 (1969) 937–946.
- [42] E. Ruckenstein, C. Berbente, The occurrence of interfacial turbulence in the case of diffusion accompanied by chemical reaction, *Chem. Eng. Sci.* 19 (1964) 329–347.
- [43] D.R. Olander, L.B. Reddy, The effect of concentration driving force on liquid–liquid mass transfer, *Chem. Eng. Sci.* 19 (1964) 67–73.
- [44] C.V. Sternling, L.E. Scriven, Interfacial turbulence—hydrodynamic instability and the Marangoni effect, *AIChE J.* 5 (1959) 514–523.
- [45] J.R.A. Pearson, On convection cells induced by surface tension, *J. Fluid Mech.* 4 (1958) 489–500.
- [46] T.K. Sherwood, J.C. Wei, Interfacial phenomena in liquid extraction, *Ind. Eng. Chem.* 49 (1957) 1030–1034.
- [47] V.G. Levich, *Physicochemical Hydrodynamics*, Prentice Hall Inc., Englewood Cliffs, NJ, 1962.
- [48] Dow, Optim™ synthetic glycerine—viscosity, <<http://www.dow.com/safechem/optim/optim-advantage/physical-properties/viscosity.htm>>, (accessed 09.02.12).
- [49] Surface tension values of some common test liquids for surface energy analysis, <<http://www.surface-tension.de/>>, (accessed 09.02.12).